

Mass-gap Black Holes in Coalescing Neutron Star Black Hole Binaries

Zepei Xing^{1,2,4,*}, Vicky Kalogera^{3,4}, Tassos Fragos^{1,2}, Jeff J. Andrews⁵, Simone S. Bavera^{1,2}, Max Briel^{1,2}, Seth Gossage⁴, Konstantinos Kovlakas^{6,7}, Matthias U. Kruckow^{1,2}, Kyle A. Rocha^{3,4}, Meng Sun⁴, Philipp M. Srivastava^{3,8}, Emmanouil Zapartas⁹

¹ Département d’Astronomie, Université de Genève, Chemin Pegasi 51, CH-1290 Versoix, Switzerland

² Gravitational Wave Science Center (GWSC), Université de Genève, CH1211 Geneva, Switzerland

³ Department of Physics & Astronomy, Northwestern University, 2145 Sheridan Road, Evanston, IL 60208, USA

⁴ Center for Interdisciplinary Exploration and Research in Astrophysics (CIERA), 1800 Sherman, Evanston, IL 60201, USA

⁵ Department of Physics, University of Florida, 2001 Museum Rd, Gainesville, FL 32611, USA

⁶ Institute of Space Sciences (ICE, CSIC), Campus UAB, Carrer de Magrans, 08193 Barcelona, Spain

⁷ Institut d’Estudis Espacials de Catalunya (IEEC), Carrer Gran Capità, 08034 Barcelona, Spain

⁸ Electrical and Computer Engineering, Northwestern University, 2145 Sheridan Road, Evanston, IL 60208, USA

⁹ Institute of Astrophysics, FORTH, N. Plastira 100, Heraklion, 70013, Greece

Received XXYZZ; Accepted XXYZZ

ABSTRACT

The existence of a mass gap of $3 - 5 M_{\odot}$ between the heaviest neutron stars (NSs) and the lightest black holes (BHs), inferred from the BH mass distribution in low mass X-ray binaries (LMXBs), has been suggested for decades. The recently reported gravitational-wave source GW230529 has been confidently identified as a neutron star–black hole (NSBH) merger, with the BH mass falling within this lower mass gap. This detection provides strong evidence against the existence of the latter and introduces new implications for the coalescing NSBH population, including a revised BH mass distribution and an updated local merger rate. In this study, we employ POSYDON, a binary population synthesis code that integrates detailed single- and binary-star models, to investigate coalescing NSBH binaries formed through isolated binary evolution. In particular, we focus on the BH mass distribution of the intrinsic NSBH merger population. We find that, with a high common-envelope efficiency of $\alpha_{\text{CE}} = 2$, the BH masses in NSBH mergers concentrate in the lower mass gap, aligning more closely with observations. However, after accounting for the constraints of the selection bias against mass-gap BHs in LMXBs, which suggests that the maximum NS birth mass is below $\approx 2 M_{\odot}$, we find that introducing a high α_{CE} is not required to match observations. Additionally, we explore the impact of core-collapse supernova kicks on the BH mass distribution and the local merger rate density of NSBH mergers. Finally, we present the property distributions of observable NSBH mergers from our simulation and find that they match well with the observations. With a self-consistent estimate of BH spins, we find that the fraction of electromagnetic counterparts in observable populations is $\approx 4 - 30\%$, depending on different NS equations of state. Future detections of coalescing NSBH binaries would provide invaluable insights into SN mechanisms, common envelope evolution, and NS physics.

Key words. Gravitational waves – Stars: neutron – Stars: black holes – binaries: close

1. Introduction

The first observation consistent with masses for neutron star–black hole (NSBH) merger events was announced by Abbott et al. (2021a) in 2021. The event, GW200105, has component masses $M_{\text{BH}} = 8.9^{+1.2}_{-1.5} M_{\odot}$ and $M_{\text{NS}} = 1.9^{+0.3}_{-0.2} M_{\odot}$, and effective inspiral spin parameter $\chi_{\text{eff}} = -0.01^{+0.11}_{-0.15}$, strongly peaking around zero. The other event, GW200115, has component masses $M_{\text{BH}} = 5.7^{+1.8}_{-2.1} M_{\odot}$ and $M_{\text{NS}} = 1.5^{+0.7}_{-0.3} M_{\odot}$, and effective inspiral spin parameter $\chi_{\text{eff}} = -0.19^{+0.23}_{-0.35}$. The possible negative χ_{eff} suggests the BH spin is antialigned with the orbit. However, Mandel & Smith (2021) later argued that a nonspinning BH is more consistent with astrophysical understanding. From these two events, Abbott et al. (2021a) inferred a local merger rate density of $\mathcal{R}_{\text{NSBH}} = 45^{+75}_{-33} \text{Gpc}^{-3} \text{yr}^{-1}$.

In April 2024, Abac et al. (2024) reported a detection of a NSBH merger event, GW230529, during the forth observing

run of LIGO, Virgo, and KAGRA (LVK) network. The primary mass of GW230519 is estimated to be $3.6^{+0.8}_{-1.2} M_{\odot}$ and the secondary mass is $1.4^{+0.6}_{-0.2} M_{\odot}$. The effective inspiral-spin χ_{eff} is measured to be $-0.10^{+0.12}_{-0.17}$, which suggests either an anti-aligned spin component or negligible spins. The χ_{eff} is correlated with the mass ratio $q = M_{\text{NS}}/M_{\text{BH}}$, with more negative χ_{eff} corresponding to a more comparable mass ratio. Including the new event GW230529, Abac et al. (2024) updated the inferred local merger rate density to $\mathcal{R}_{\text{NSBH}} = 85^{+116}_{-57} \text{Gpc}^{-3} \text{yr}^{-1}$.

Prior to gravitational wave (GW) observations, the BH mass distribution inferred from the X-ray binary populations indicated a low-mass boundary of $\approx 5 M_{\odot}$ (Bailyn et al. 1998; Özel et al. 2010; Farr et al. 2011). In the meantime, the maximum NS mass has been suggested to be below $\approx 2.4 M_{\odot}$ based on X-ray and radio observations (Linares et al. 2018; Kandel & Romani 2020; Romani et al. 2022), below $\approx 2.52 M_{\odot}$ from GW observations (Abbott et al. 2020a), and below $\approx 3 M_{\odot}$ based on theoretical constraints (Rhoades & Ruffini 1974; Kalogera & Baym 1996;

* e-mail: Zepei.Xing@unige.ch

Godzieba et al. 2021). The lightest BH and the heaviest NS lead to a mass gap of $\sim 3-5 M_{\odot}$. Several candidate systems have been suggested to contain a BH in the mass gap from electromagnetic observations (Zdziarski et al. 2013; Heida et al. 2017; Thompson et al. 2019; Casares et al. 2022) and from GW detections (Abbott et al. 2020c, 2021b, 2023, 2024), but none have been confirmed with high confidence. Fryer et al. (2012) built two analytical supernova (SN) prescriptions based on different assumptions of the instability growth timescale to map the carbon-oxygen core mass to compact object remnant mass. With the rapid prescription, the mass gap can be generated, while the delayed prescription predicts a continuous remnant mass distribution. No theoretical constraints are able to determine which one is more representative.

GW230529 is the first detection of a compact binary whose primary component is highly likely to fall within the mass gap, potentially resolving the longstanding debate on the existence of the mass gap. Assuming that the range of $3-5 M_{\odot}$ represents the mass gap, Abac et al. (2024) provided a merger rate for binaries with components within the gap of $\mathcal{R}_{\text{gap}} = 24^{+28}_{-16} \text{ Gpc}^{-3} \text{ yr}^{-1}$ or $\mathcal{R}_{\text{gap}} = 33^{+89}_{-29} \text{ Gpc}^{-3} \text{ yr}^{-1}$ based on two different population models. A key question is why the mass-gap BHs are hidden in the low mass X-ray binary (LMXB) population. Siegel et al. (2023) investigated selection biases against mass-gap BHs, taking into account that a dynamical BH mass measurement requires the existence of transient behaviors of the corresponding LMXBs. They found that with rapid population synthesis simulations, all model combinations predict detection of LMXBs containing mass-gap BHs. However, using detailed binary stellar-evolution models, they found that observational biases against mass-gap BHs appear when the maximum NS birth mass is less than $\approx 2 M_{\odot}$. If the maximum NS birth mass is greater, the mass gap would be filled by BHs formed through accretion induced collapse in LMXBs and we should have observed plenty of them.

In this study, we use the binary population synthesis code POSYDON (Fragos et al. 2023), which incorporates extensive grids of detailed stellar binary-evolution models, to study the formation of coalescing NSBH systems across the Universe. Particularly, we focus on the BH mass distributions of coalescing NSBHs and the effects of model variations of common envelope (CE) evolution and SN kicks. With POSYDON, we are able to self-consistently estimate the BH spins and, thus, more accurately infer the fraction of associated electromagnetic counterparts.

2. Methods

To simulate populations of binaries, we employ an updated version (v2.0) of the publicly available code POSYDON¹ (Andrews et al. in prep.), which integrates detailed single- and binary-star model grids, simulated using the stellar evolution code Modules for Experiments in Stellar Astrophysics (MESA, Paxton et al. 2011, 2013, 2015, 2018, 2019; Jermyn et al. 2023). Compared to POSYDON v1.0 (Fragos et al. 2023), POSYDON v2.0 extends to include grids with eight metallicities $Z = 0.0001, 0.001, 0.01, 0.1, 0.2, 0.45, 1, 2 Z_{\odot}$.

We evolve a population of 10^6 binaries for each metallicity, starting from two zero-age main-sequence stars. We sample the primary mass following the initial mass function from Kroupa (2001), within the range of $7-120 M_{\odot}$. The secondary

mass, ranging from $0.5 M_{\odot}$ to $120 M_{\odot}$, adheres to a flat distribution from the minimal ratio to 1 with respect to the primary mass. The initial orbital periods follow the distribution of Sana et al. (2013) from 1 days to 6000 days. We extend it to 0.35 days with a logarithmic uniform distribution. We assume the initial orbits are circular and the two stars are tidally synchronized. For all the population models presented in this study, we employed the nearest-neighbor interpolation scheme to interpolate between models in the binary grids (see Section 7 in Fragos et al. 2023).

To calculate the compact object masses through core-collapse supernova (CCSN), we adopted the Fryer et al. (2012) delayed prescription, which allows the formation of mass-gap BHs. Regarding the CCSN natal kick velocity for NSs, we adopt a Maxwellian distribution with a velocity dispersion of $\sigma_{\text{CCSN}} = 265 \text{ km s}^{-1}$ (Hobbs et al. 2005). Some studies have implied that the NS kick should be weaker. For example, O’Doherty et al. (2023) obtained a velocity dispersion of $\sigma_{\text{CCSN}} = 61.6 \text{ km s}^{-1}$ from the populations of NS binaries. It should be considered as the lower limit because their sample excludes the disrupted systems where the NSs received large kicks. As a result, we also consider $\sigma_{\text{CCSN}} = 61.6 \text{ km s}^{-1}$ and a moderate value of $\sigma_{\text{CCSN}} = 150 \text{ km s}^{-1}$ for the purpose of parameter study. BH kicks follow the same distribution but rescaled by a factor of $1.4 M_{\odot}/M_{\text{BH}}$.

In POSYDON, the maximum NS mass is, by default, set to be $2.5 M_{\odot}$. To account for selection biases against mass-gap BHs in LMXBs, we also consider a maximum NS birth mass of $M_{\text{NS,birth-max}} = 2 M_{\odot}$ (Siegel et al. 2023). To achieve this, we assume that all compact objects born with masses above $2 M_{\odot}$ as predicted by the delayed prescription, are light BHs instead of NSs. This assumption excludes these binaries from the NSBH populations. We acknowledge that we do not include a self-consistent SN prescription for classifying remnant type and predicting the masses of these specific compact objects. A small population of double NSs with one of the NS heavier than $2 M_{\odot}$ at birth would turn to NSBHs based on this assumption about the NS maximum birth mass. In our populations, the contribution of these systems is insignificant.

Utilizing the stellar profiles of the BH progenitors at carbon depletion, we calculate the BH spins by following the method described in the Appendix D of Bavera et al. (2021). We assume that the BH spin vector is the same as that of its progenitor, and that the progenitor is always aligned with the orbit. We ignore any change in the BH spin direction due to mass transfer. The final orbital tilt is the combination of two tilts originating from two SN kicks (Xing et al. 2024). We take into account the change of BH spin magnitude due to accretion. However, it has limited effects because we applied Eddington-limited accretion.

For the CE evolution, we employ the α - λ prescription (Webbink 1984; de Kool et al. 1987; Livio & Soker 1988). The CE efficiency parameter α_{CE} determines how efficient the energy can be utilized to expel the envelope. By default, we set $\alpha_{\text{CE}} = 1$. The parameter λ_{CE} depends on the mass and the internal structure and energy profile of the stars at the onset of CE evolution (Dewi & Tauris 2000). Unlike most rapid BPS codes, which use pre-tabulated λ_{CE} values obtained from studies on single stars, POSYDON allows for on-the-fly calculations of λ_{CE} based on the profiles of the stars. To determine the boundary of the helium core and the envelope, we select the layer where the hydrogen mass fraction $X_{\text{H}} = 0.1$ by default (see Section 8.2 in Fragos et al. 2023).

From the simulated binaries, we select those binaries forming a NS and a BH that would merge within a Hubble time to comprise our synthetic population. Then, we distribute the syn-

¹ We utilized the version of the POSYDON code identified by the commit hash 5acad13, available at <https://github.com/POSYDON-code/POSYDON/>, along with the POSYDON v2.0 dataset will be published here: <https://zenodo.org/communities/posydon>.

thetic population across the cosmic history of the Universe at every Δt_i (100 Myr by default) cosmic time interval centered on the redshift z_i (see Appendix D in [Bavera et al. 2022](#)). To account for the metallicity- and redshift-dependent star formation history (SFH), for each coalescing NSBH system, we calculate its cosmological weight based on the star formation rate density and metallicity distribution from the TNG100 Illustris large-scale cosmological simulation ([Nelson et al. 2019](#)). Then, the weighted population represents the intrinsic population. Finally, we calculate the detection probability p_{det} for each binary assuming a network of LIGO-Hanford, LIGO-Livingston, and Virgo at design sensitivity (see [Abbott et al. 2020b](#)) to generate the observable populations.

3. Results

3.1. The Role of Common Envelope Efficiency

In Figure 1, we show the distribution of BH and NS masses for the intrinsic populations in our simulations, with $\alpha_{\text{CE}} = 1$ on the left and $\alpha_{\text{CE}} = 2$ on the right. Additionally, we present the 1D BH mass distributions and compare them with the distribution inferred from the three events GW230529, GW200105, and GW200115 ([Abac et al. 2024](#)). We also show the contributions from two main formation channels that we defined: channel CE, for which the binary experiences CE evolution either before or after the BH formation, and channel SMT, where the binary undergoes at least one stable mass transfer phase without any CE evolution. In channel CE, the classical pathway dominates, where the two non-degenerate stars undergo stable mass transfer, and after the primary star forms a BH, the secondary star and the BH initiate a CE phase. More frequently, the binary experiences a subsequent case BB mass transfer, where the secondary helium star expands to fill the Roche lobe due to shell helium burning. In channel SMT, most binaries undergo two stable mass transfer phases, one before and one after the BH formation. Some binaries avoid mass transfer before BH formation and experience stable mass transfer afterward.

Utilizing our default parameter settings, with $\alpha_{\text{CE}} = 1$, we can see two prominent peaks: one around $M_{\text{BH}} \approx 4 - 5 M_{\odot}$ and $M_{\text{NS}} \approx 1.3 M_{\odot}$, and another at $M_{\text{BH}} \approx 7 - 8 M_{\odot}$ and $M_{\text{NS}} \approx 2.1 - 2.2 M_{\odot}$. The paucity of NSs around $\sim 1.7 M_{\odot}$ is caused by the discontinuity of $0.1 M_{\odot}$ in the proto-compact object mass equation at carbon-oxygen core masses of $3.5 M_{\odot}$ in the [Fryer et al. \(2012\)](#) delayed prescription, which was also discussed in [Broekgaarden et al. \(2021\)](#). The compact object mass depends on not only the initial progenitor mass, but also mass transfer process during the evolution, which affects the final core mass of the progenitor at core-collapse. Especially for NSs, case BB mass transfer plays a crucial role, as the amount of mass remaining after this mass transfer phase directly determines the NS mass. Massive NSs typically originate from helium stars that do not lose much mass through case BB mass transfer or avoid it. If the NS progenitor loses mass to end up with a final helium core in the mass range of $1.4 - 2.5 M_{\odot}$ ([Podsiadlowski et al. 2004](#)), it will form a NS of $\approx 1.26 M_{\odot}$ through electron-capture SN. If the NS progenitor has a final carbon-oxygen core mass below $2.5 M_{\odot}$, based on the [Fryer et al. \(2012\)](#) delayed prescription, it will eventually become a NS of $\approx 1.27 M_{\odot}$. We can see from Figure 1 that these light NSs have a significant contribution in mass-gap NSBHs.

Notably, for the default model, the BH mass distribution shows the highest probability at $\approx 7 M_{\odot}$, not in agreement with the observation. In contrast, when adopting a larger α_{CE} of 2, the

BH mass distribution shifts towards lower masses, concentrating around $\approx 4 M_{\odot}$, with a deficiency at $7 - 10 M_{\odot}$. The result is consistent with the findings of [Zhu et al. \(2024\)](#), who found a low-mass peak of $3.4 M_{\odot}$ within the mass gap when adopting $\alpha_{\text{CE}} = 2$. We find that a larger α_{CE} does not increase the merger rate of NSBHs with heavy BHs ($\gtrsim 6 M_{\odot}$) but significantly facilitates the formation of NSBHs with light BHs. The reason is that, in the underlying populations, plenty of binaries with light BHs initiated a CE phase and subsequently merged in CE evolution. Compared to binaries containing heavy BHs, they are greater in number but tend to have lower orbital energy, making it harder to eject the envelope of the companion star. Hence, a more efficient energy conversion in CE evolution would substantially increase the number of systems succeeding in CE evolution with light BHs in particular. Additionally, some binaries with heavy BHs would result in wider orbits due to a larger α_{CE} , and would no longer merge within a Hubble time. The fraction of channel CE increase from $\approx 70\%$ for $\alpha_{\text{CE}} = 1$ to $\approx 86\%$ for $\alpha_{\text{CE}} = 2$. The mass-gap NSBHs are largely from channel CE.

Although a larger α_{CE} provides a better match to the observation by producing the peak within the mass gap, we see a mild deficiency in BHs with masses $\gtrsim 7 M_{\odot}$. In POSYDON, when calculating the parameter λ_{CE} , we integrate both the gravitational energy and internal energy of the envelope, subtracting the recombination energy. As a result, we are inclined to adopt α_{CE} values not greater than 1, as no other energy source is evident to justify a large α_{CE} of 2.

3.2. Supernova Natal Kicks

In this section, we investigate the impact of SN kicks on the BH mass distributions of coalescing NSBH binaries. In Figure 2 we show the distribution of BH and NS masses in coalescing NSBH populations for another two different SN kick velocities of $\sigma_{\text{CCSN}} = 150 \text{ km s}^{-1}$ and $\sigma_{\text{CCSN}} = 61.6 \text{ km s}^{-1}$. The populations are generated using $\alpha_{\text{CE}} = 1$. We can see that a lower kick velocity of $\sigma_{\text{CCSN}} = 150 \text{ km s}^{-1}$ does not significantly alter the BH mass distribution but only slightly increase the fraction of lower mass-gap BHs compared to the default $\sigma_{\text{CCSN}} = 265 \text{ km s}^{-1}$ shown in Figure 1. In the case of $\sigma_{\text{CCSN}} = 61.6 \text{ km s}^{-1}$, the peak shifts toward lower BH masses and the channel CE becomes completely dominant. This occurs because the underlying population favors light BHs going through CE evolution, and weak kicks prevent these binaries from being disrupted. Moreover, binaries going through SMT typically require high eccentricities induced by strong kicks to merge within a Hubble time. As a result, weak kicks reinforce the dominance of channel CE. The fraction of channel CE is 75% and 97% for $\sigma_{\text{CCSN}} = 150 \text{ km s}^{-1}$ and $\sigma_{\text{CCSN}} = 61.6 \text{ km s}^{-1}$, respectively.

Although lower kick velocities slightly raise the percentage of lower mass-gap BHs, the overall distribution does not align well with the observation. For $\sigma_{\text{CCSN}} = 61.6 \text{ km s}^{-1}$, the fraction of NSBH mergers with BH masses above $\approx 11 M_{\odot}$ becomes marginal. Furthermore, this low kick velocity increases the local merger rate density of NSBHs to an excessively high value. We estimate the local merger rate density of NSBH mergers for varied kick velocities at redshift zero. The three kick velocities $\sigma_{\text{CCSN}} = 265 \text{ km s}^{-1}$, $\sigma_{\text{CCSN}} = 150 \text{ km s}^{-1}$, and $\sigma_{\text{CCSN}} = 61.6 \text{ km s}^{-1}$ correspond to local merger rate densities of $72 \text{ Gpc}^{-3} \text{ yr}^{-1}$, $193 \text{ Gpc}^{-3} \text{ yr}^{-1}$, and $408 \text{ Gpc}^{-3} \text{ yr}^{-1}$, respectively. The rate for the lowest kick velocity, $\sigma_{\text{CCSN}} = 61.6 \text{ km s}^{-1}$, is significantly higher than the upper limit of the NSBH local merger rate estimated from LVK analysis.

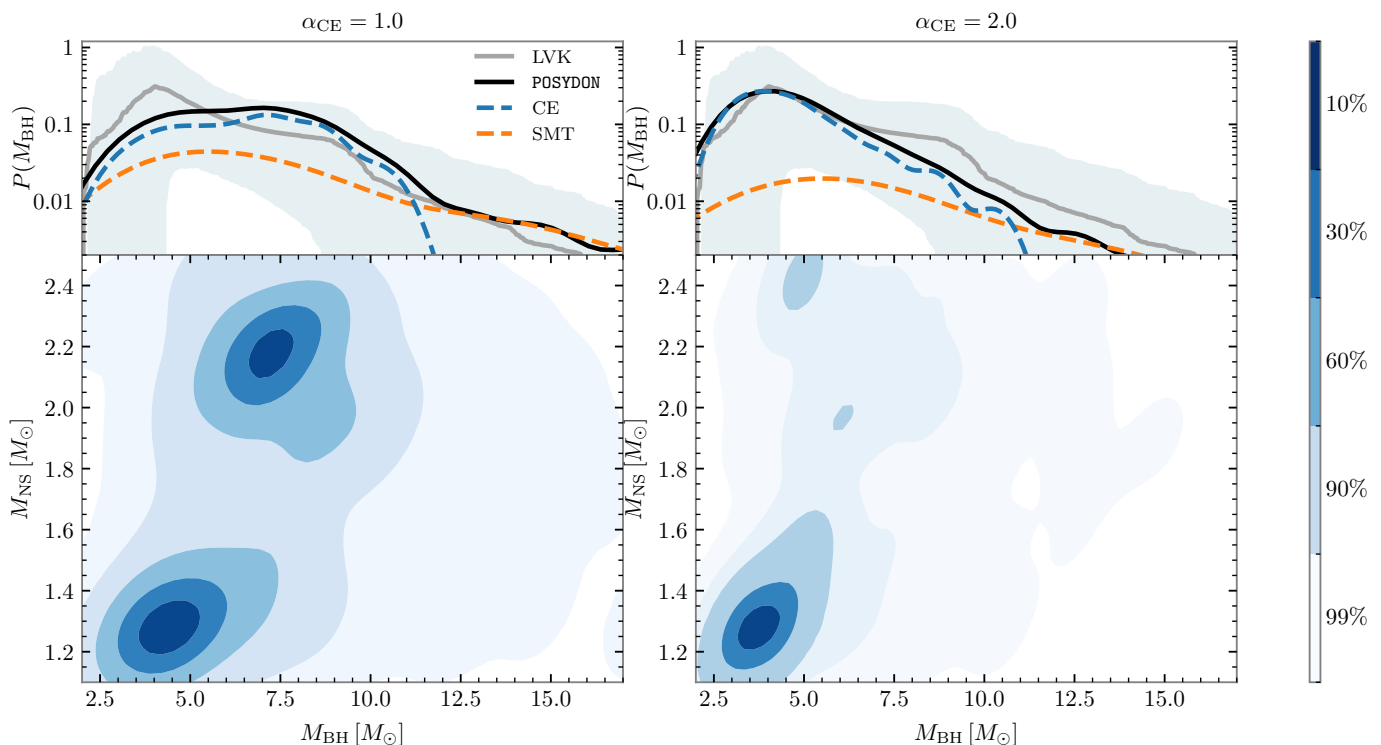


Fig. 1. NS and BH mass distributions of our intrinsic coalescing NSBH populations. Left and right panels correspond to the populations generated with CE parameter $\alpha_{\text{CE}} = 1$ and 2, respectively. The top panels show the BH mass distributions inferred from the three detected events in grey line with 90% credible interval in teal shaded region and from our population model in black line. The contributions from channel CE and channel SMT are in blue dashed line and orange dashed line, respectively. The bottom panels show the kernel density estimate plot of component masses ranging from 1% to 90% credible interval region.

3.3. Account for the Mass-Gap Black Holes in Low Mass X-ray Binaries

In this section, we consider the constraints on the maximum NS birth mass. Following the investigation of selection bias against mass-gap BHs in the LMXB population (Siegel et al. 2023), we exclude binaries with NS birth masses exceeding the maximum value of $2 M_{\odot}$ from our intrinsic population. Figure 3 shows the distributions of NS and BH masses from the same populations presented in Figure 1 and Figure 2, but with the maximum NS birth mass set to $2 M_{\odot}$. With this restriction, we can see that the default setting with $\alpha_{\text{CE}} = 1$ and $\sigma_{\text{CCSN}} = 265 \text{ km s}^{-1}$ also predicts a prominence of BH masses around the high-end edge of the lower mass gap. The number of high-mass BHs around $7 M_{\odot}$ is reduced, as most of them are paired with high-mass NSs above $2 M_{\odot}$, which are removed from the population. Now, a higher $\alpha_{\text{CE}} = 2$ predicts an overabundance of mass-gap BHs, particularly BHs lighter than $\approx 4 M_{\odot}$, and a paucity of BHs with mass above $\approx 7 M_{\odot}$. Less than $\approx 10\%$ of coalescing NSBH systems contain BHs outside the mass gap. In this case, the coalescing NSBHs containing BHs more massive than $\approx 7.5 M_{\odot}$ are formed through channel SMT. Both models with lower kick velocities predict a BH mass peak within $4 - 5 M_{\odot}$. The moderate kick velocity $\sigma_{\text{CCSN}} = 150 \text{ km s}^{-1}$ exhibits the best match to the BH mass distribution inferred from the observation regarding the peak and the tail for massive BHs.

The local merger rate densities of NSBHs and mass-gap NSBHs for all the model variations are summarized in Table 1. With the restriction on NS birth mass, \mathcal{R}_{gap} barely changes, as mass-gap BHs are accompanied by low-mass NSs. With $M_{\text{NS, birth-max}} = 2 M_{\odot}$, the three kick velocities $\sigma_{\text{CCSN}} =$

265 km s^{-1} , $\sigma_{\text{CCSN}} = 150 \text{ km s}^{-1}$, and $\sigma_{\text{CCSN}} = 61.6 \text{ km s}^{-1}$ correspond to local merger rate densities of $40 \text{ Gpc}^{-3} \text{ yr}^{-1}$, $119 \text{ Gpc}^{-3} \text{ yr}^{-1}$, and $274 \text{ Gpc}^{-3} \text{ yr}^{-1}$, respectively. The lowest kick velocity $\sigma_{\text{CCSN}} = 61.6 \text{ km s}^{-1}$ still predicts a merger rate density exceeding the upper limit of the updated rate inferred from the three events. This is reasonable as the velocity should be considered as a lower limit (O’Doherty et al. 2023). In the other two cases, the predicted merger rates are consistent with the inferred merger rates.

3.4. Observable Population

In the previous sections, we presented BH and NS mass distributions of the intrinsic coalescing NSBH populations in our simulations, which are not directly comparable to observed events. In Figure 4, we display the properties of the observable population for the model of $\alpha_{\text{CE}} = 1$, $M_{\text{NS, birth-max}} = 2 M_{\odot}$, and $\sigma_{\text{CCSN}} = 150 \text{ km s}^{-1}$, including the distributions of the BH mass, NS mass, mass ratio, and the BH spin at the direction of the orbit $\chi_{\text{BH,z}}$. We also display the properties of the three observed events in the figure. We can see that our simulation can match the properties of the three events well. A higher detection probability for BHs around $\approx 7 M_{\odot}$ and NSs around $\approx 1.9 M_{\odot}$ appears, which is consistent with the event GW200105, with respect to the intrinsic population. The mass ratio distribution centers at ≈ 0.2 and can barely reach 0.5. The $\chi_{\text{BH,z}}$ is centered at zero, with a spread to ≈ 0.1 and a small bump at ≈ 0.25 . Most BHs have negligible natal spins because BH progenitors lose most of their angular momentum through mass transfer and winds. The small bump at ≈ 0.25 corresponds to initially close binaries where tides can

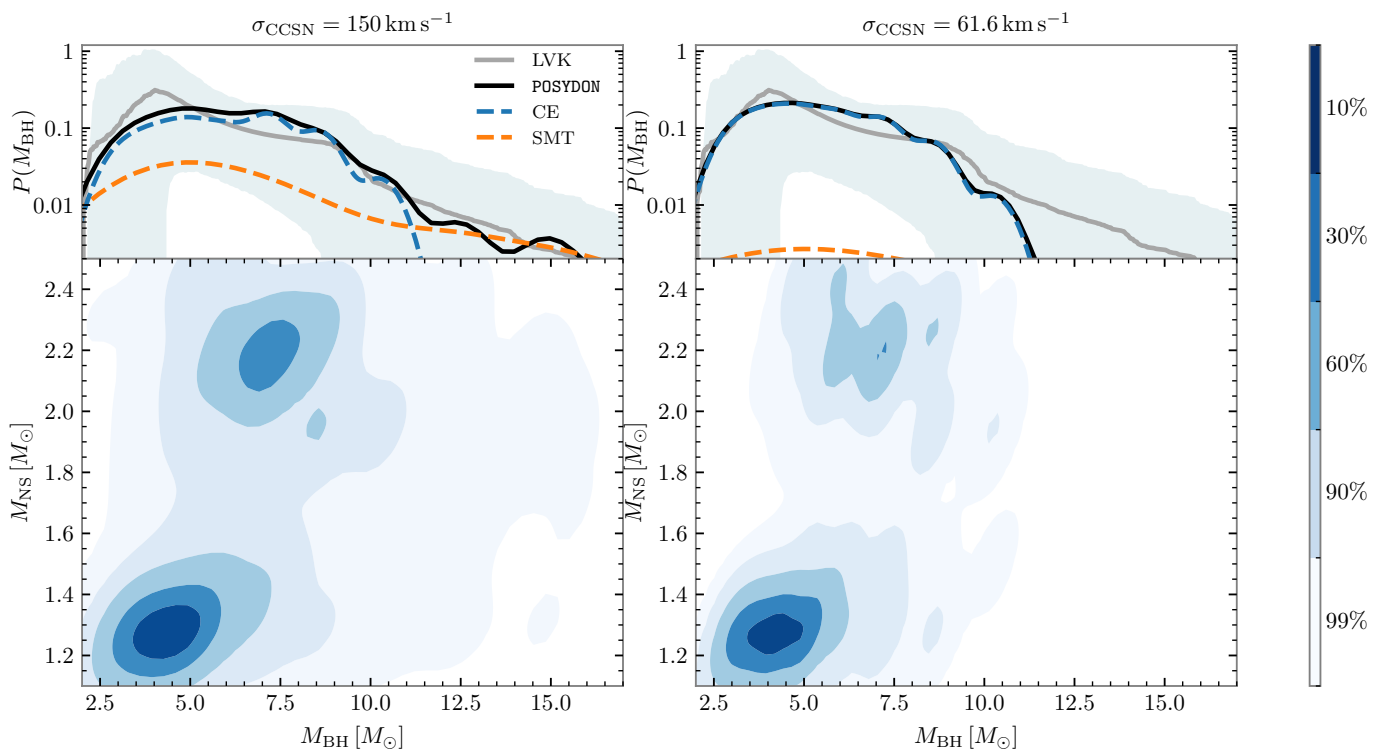


Fig. 2. Same as Figure 1 with $\alpha_{\text{CE}}=1$, but with different kick velocities of $\sigma_{\text{CCSN}} = 150$ and 61.6 km s^{-1} .

Table 1. Local Merger Rate Density of NSBH Mergers for Different Models

Model	$\mathcal{R}_{\text{NSBH}}[\text{Gpc}^{-3}\text{yr}^{-1}]$	$\mathcal{R}_{\text{gap}}[\text{Gpc}^{-3}\text{yr}^{-1}]$
POSYDON default	72	11
$\alpha_{\text{CE}} = 2$	162	57
$\sigma_{\text{CCSN}} = 150 \text{ km s}^{-1}$	193	41
$\sigma_{\text{CCSN}} = 61.6 \text{ km s}^{-1}$	408	105
$M_{\text{NS,birth-max}} = 2 M_{\odot}$	40	10
$\alpha_{\text{CE}} = 2, M_{\text{NS,birth-max}} = 2 M_{\odot}$	110	55
$\sigma_{\text{CCSN}} = 150 \text{ km s}^{-1}, M_{\text{NS,birth-max}} = 2 M_{\odot}$	119	40
$\sigma_{\text{CCSN}} = 61.6 \text{ km s}^{-1}, M_{\text{NS,birth-max}} = 2 M_{\odot}$	274	103

Notes. Inferred rates from LVK: $\mathcal{R}_{\text{NSBH}} = 85^{+116}_{-57} \text{ Gpc}^{-3}\text{yr}^{-1}$ and $\mathcal{R}_{\text{gap}} = 24^{+28}_{-16} \text{ Gpc}^{-3}\text{yr}^{-1}$ or $33^{+89}_{-29} \text{ Gpc}^{-3}\text{yr}^{-1}$ (Abac et al. 2024).
 POSYDON default: $\alpha_{\text{CE}} = 1, M_{\text{NS,birth-max}} = 2.5 M_{\odot}, \sigma_{\text{CCSN}} = 265 \text{ km s}^{-1}$

spin up the BH progenitors. Because we assume that BH accretion is Eddington-limited, the accretion spin-up is not significant. The BHs can be spun up by case BB mass transfer but the increase is typically below 0.1. BH spins as high as ≈ 0.5 are attributed to stable case A mass transfer, but the fraction of such cases is negligible. The three events are consistent with nearly zero $\chi_{\text{BH,z}}$. For GW230529, if its primary compact object is a massive NS, as the mass ratio is anti-correlated with the primary mass, the secondary NS is expected to be massive at birth, even exceeding the threshold of $2 M_{\odot}$. If its primary is a BH, it is more likely that the BH mass is at the higher end.

3.5. Electromagnetic Counterparts

To estimate the fraction of potential associated electromagnetic counterparts (EMCs) in NSBH mergers, we utilize the empirical formula provided by Foucart et al. (2018) to calculate the remnant mass outside the innermost stable circular orbit (ISCO) of the BH resulting from the tidal disruption of the NS. The systems having non-zero remnant mass outside ISCO are considered to produce EMCs such as short gamma-ray bursts and kilonovae. We assume three NS radii $R_{\text{NS}} = 11 \text{ km}, 12 \text{ km},$ and 13 km , encompassing a range of NS equations of state from soft to stiff. For the default model with $\alpha_{\text{CE}} = 1$ and $\sigma_{\text{CCSN}} = 265 \text{ km s}^{-1}$, we obtain EMC fractions for the intrinsic population of 3%, 16%, and 26% for $R_{\text{NS}} = 11 \text{ km}, 12 \text{ km},$ and 13 km , respectively. In our preferred model, with $\alpha_{\text{CE}} = 1, \sigma_{\text{CCSN}} = 150 \text{ km s}^{-1}$, and

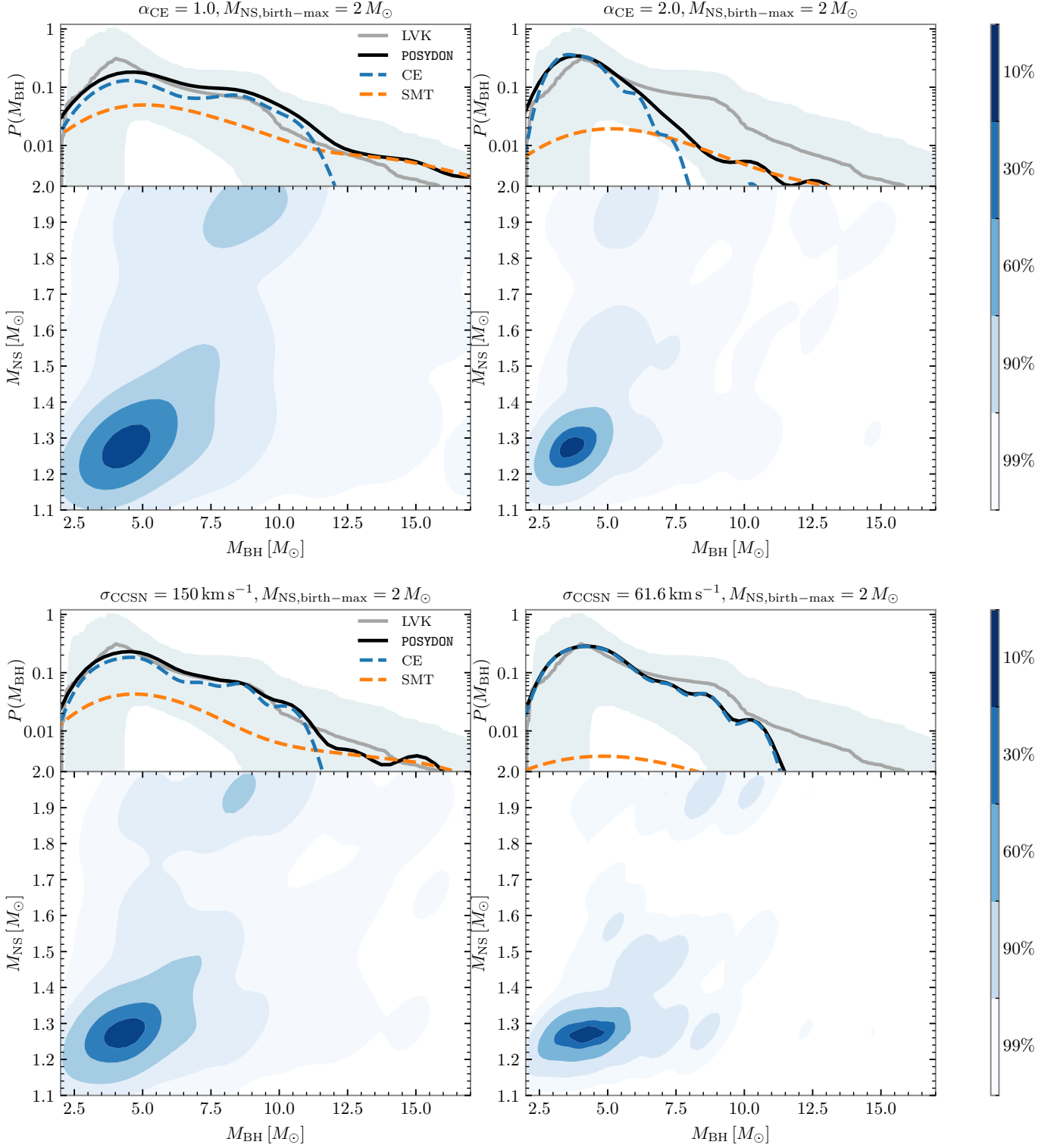


Fig. 3. NS and BH mass distributions of our intrinsic coalescing NSBH population, assuming the maximum NS birth mass is $2 M_{\odot}$.

$M_{\text{NS,birth-max}} = 2 M_{\odot}$, the fractions increase to 11%, 36%, and 57%. The EMC fractions increase substantially because the preferred model predicts a larger fraction of systems with light BHs and light NSs, which increase the chance of tidal disruption for the NSs outside the ISCO.

Shifting from the intrinsic to the observable populations, we estimate the EMC fractions for observable systems. The default model yields EMC fractions of 1%, 6%, and 10% for

$R_{\text{NS}} = 11 \text{ km}$, 12 km , and 13 km , respectively. Under our preferred model, we find EMC fractions of 4%, 20%, and 31%. The detection of GW230529 shifts the BH mass distributions toward lower masses in NSBH merger populations, leading to an increased chance of observing associated EMCs, especially if the NS equation of state is stiff.

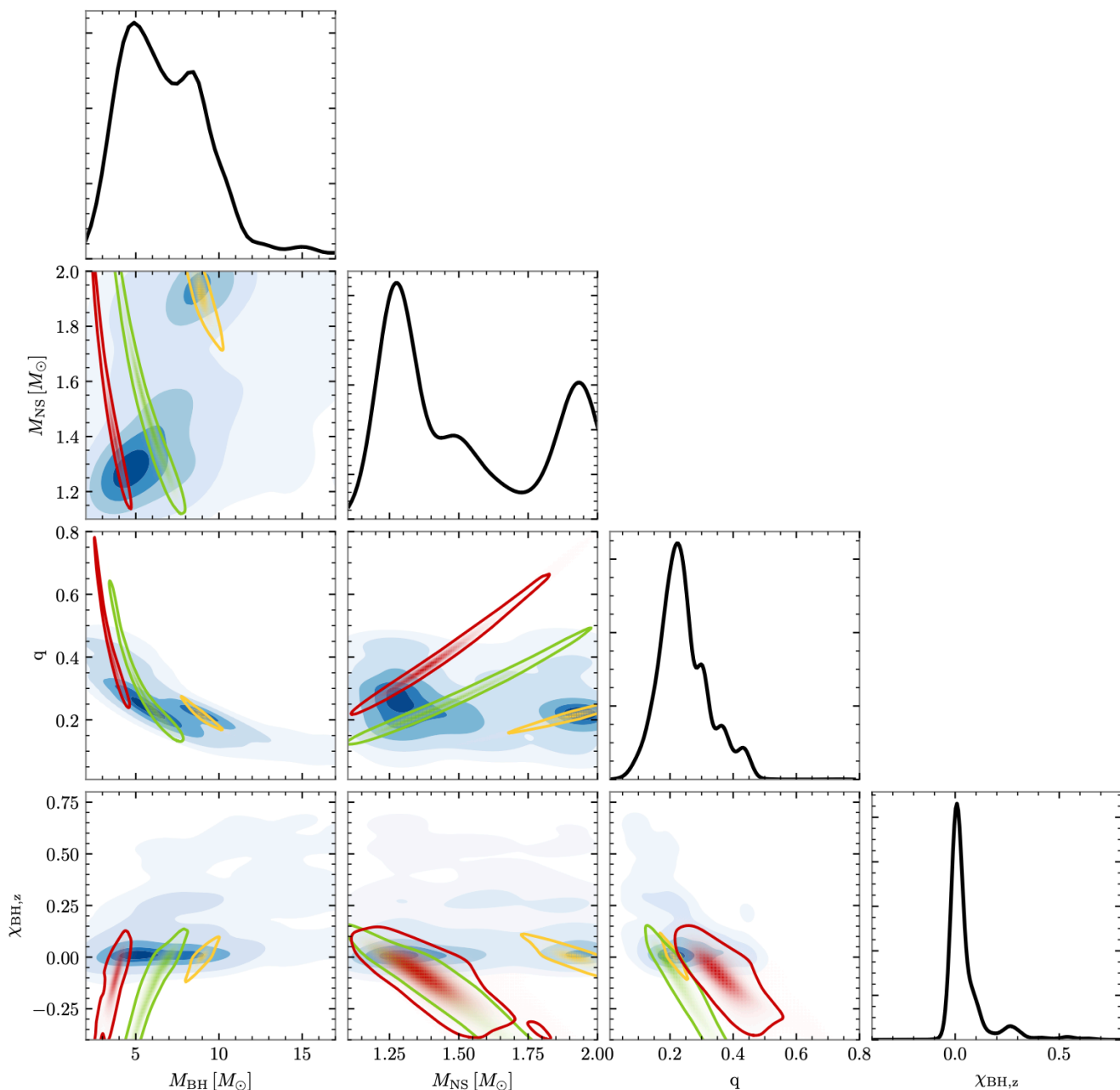


Fig. 4. Corner plot of the observable population of coalescing NSHBs in our simulation, generated with $\alpha_{\text{CE}} = 1$, $\sigma_{\text{CCSN}} = 150 \text{ km s}^{-1}$ and $M_{\text{NS,birth-max}} = 2 M_{\odot}$. We show the BH mass, NS mass, mass ratio, and BH spin component parallel to the direction of the orbital plane. The red, green, and yellow contours indicate the 90% confidence interval of GW230529, GW200115, and GW200105, respectively.

4. Discussion

4.1. Uncertainties

One of the primary uncertainties in our BPS study is the SN prescription, specifically the association between pre-SN progenitor core masses and the compact object masses. The Fryer et al. (2012) delayed prescription allows for mapping compact objects within the lower-mass gap. However, the discontinuity in NS mass around $1.7 M_{\odot}$ is neither supported by the observations nor motivated by SN physics. Furthermore, the restriction on the maximum NS birth mass cannot be reconciled self-consistently with the Fryer et al. (2012) delayed prescription, suggesting a potential need for a different relationship between heavy helium or carbon-oxygen core masses and compact ob-

ject masses. Prescriptions that link the progenitor’s helium or carbon-oxygen core properties to the outcome compact object remnant properties play a key role in modeling BH and NS mass distributions in population studies and determining the fraction of associated EMCs. Future observations of double compact object mergers will put further constraints on SN prescriptions and advance our understanding of SN physics.

The models of metallicity- and redshift-dependent SFH and the assumptions made in distributing our populations across cosmic time can affect primarily the rates but also the shapes of NSBH property distributions (Broekgaarden et al. 2021). We leave the exploration of these factors to future studies when the data sample grows large enough for aiding to allow for a proper statistical comparison. Furthermore, investigating varia-

tions in stellar physics like the wind prescriptions and overshooting parameters, and in binary physics like the mass transfer efficiency is beyond the scope of this study, as changing these model assumptions would require constructing new binary simulation grids. However, the POSYDON framework allows for potential future investigations into these key physics self-consistently and precisely by integrating new grids of detailed binary models.

4.2. Maximum Neutron Star Birth Mass

Several massive NSs has been found with mass exceeding $2 M_{\odot}$, for example PSR J2215+5135 with $M_{\text{NS}} = 2.27^{+0.17}_{-0.15} M_{\odot}$ (Linares et al. 2018), PSR J0740+6620 with $M_{\text{NS}} = 2.08 \pm 0.07 M_{\odot}$ (Fonseca et al. 2021), J1810+1744 with $M_{\text{NS}} = 2.13 \pm 0.04 M_{\odot}$ (Romani et al. 2021), and PSR J0952-0607 with $M_{\text{NS}} = 2.35 \pm 0.17 M_{\odot}$ (Romani et al. 2022). All of these NSs are millisecond pulsars with a low-mass main-sequence or a white dwarf companion. They are expected to have accreted mass from their companion and been recycled. As a result, their birth masses remain unknown and could be less than $2 M_{\odot}$. In contrast, for double NSs detected in our Galaxy, the second-born NSs are typically low-mass, which can be directly interpreted as their birth mass. In the population of eclipsing NS high-mass X-ray binaries, the NSs are very young and are not expected to have accreted a significant amount of mass. In the study by Falanga et al. (2015), most NSs in high-mass X-ray binaries are measured to be below $\sim 2 M_{\odot}$, with one possible exception of Vela X-1, which contains a NS with mass $M_{\text{NS}} = 2.12 \pm 0.16 M_{\odot}$. Nevertheless, with the uncertainty in the measurement, one cannot rule out the possibility that the maximum NS birth mass is restricted around $2 M_{\odot}$.

4.3. Could NS Form First?

Xing et al. (2024) found that the BH always forms first in the population of coalescing NSBHs at solar metallicity from POSYDON simulations. This is because the rotation-dependent accretion model for non-degenerate stars in POSYDON suggests a low accretion efficiency for case B mass transfer in general, which limits the probability of mass reversal. Similar trends that low accretion efficiency for non-degenerate accretors predicting low fraction of first-born NSs in NSBH populations are also found in other population studies (Kruckow et al. 2018; Shao & Li 2021; Broekgaarden et al. 2021). Liotine et al. (in prep.) also find that POSYDON predicts low formation rate of millisecond pulsar BH binaries, where the NSs form prior to the BHs to be recycled by the BH progenitors. In some close binaries, where tides can spin down the accretor and enhance the mass accretion, rejuvenation could occur. However, the first born NSs are highly likely to enter a CE phase with massive BH progenitors and subsequently merge due to their low orbital energy (see a detailed discussion in Xing et al. 2024). In this study, we find that this conclusion also holds true for varied metallicities.

We posit that if the accretion efficiency is actually high enough to lead to mass reversal for binaries in wide orbits, the NS could form first in coalescing NSBHs. Román-Garza et al. (2021) predicted that the fraction of NSBH mergers with NS form first can reach about 10% when assuming accretion onto non-degenerate stars is limited only by the thermal timescale of the accretor, which makes the accretion efficiency much higher than the rotation-dependent accretion model. In this case, the NSs have chance to accrete mass from the BH progenitors. However, in mass transfer phases when the BH progenitors are still

hydrogen-rich stars, the large mass ratios would lead to unstable mass transfer quickly before the NS can accrete a significant amount of mass. Furthermore, if the binaries survive CE, the helium stars that are massive enough to form BHs would not experience rapid expansion, suggesting that the NSs might not have the chance to gain mass through case BB mass transfer as in LMXBs. Liotine et al. (in prep.) found that a small group of NSBHs with first-born NSs form through double CE process between two non-degenerate stars. Similarly, the NSs cannot accrete much mass from the BH progenitors. In conclusion, we expect that even if the NS forms first in coalescing NSBHs, the NS is likely to be close to its birth mass.

5. Conclusion

The detection of the new event GW230529, which very likely contains a compact object with mass in the lower mass gap, has refreshed our understanding of the coalescing NSBH populations. The inclusion of GW230529 in population inference analysis yields a new BH mass distribution for coalescing NSBHs and an updated merger rate. Most importantly, it provides strong evidence that the lower mass gap does not exist. We conduct a population synthesis study on coalescing NSBHs to investigate how the CE process and SN kick velocity affect their properties, and to reconcile the detection of mass-gap BHs from GWs with their absence in LMXBs.

We find that, using the POSYDON default model with $\alpha_{\text{CE}} = 1$, $\sigma_{\text{CCSN}} = 265 \text{ km s}^{-1}$, and $M_{\text{NS,birth-max}} = 2.5 M_{\odot}$, the BH masses are not centered within the lower mass gap as implied by observations. Increasing the CE efficiency to $\alpha_{\text{CE}} = 2$ can facilitate the formation of NSBH mergers with mass-gap BHs efficiently. These light BHs going through CE are greater in number in the underlying population, although hard in surviving CE due to low orbital energy. A higher CE efficiency would increase the success rate of CE for these light BHs, and thus lead to a surge of coalescing NSBH with mass-gap BHs. Furthermore, we find that lower kick velocities can increase the contribution of mass-gap BHs that go through CE in coalescing NSBHs. However, varying kick velocities alone is insufficient to match the BH mass distribution inferred from observations.

To explain the selection bias against mass-gap BHs in LMXBs, Siegel et al. (2023) found that a maximum NS birth mass of $\approx 2 M_{\odot}$ should be considered. With the restriction of NS birth mass in the Fryer et al. (2012) delayed prescription, we find that a large α_{CE} is not necessary for explaining the updated BH mass distribution from the analysis including GW230529. In this case, a kick velocity of $\sigma_{\text{CCSN}} = 150 \text{ km s}^{-1}$ can better match the BH mass distribution compared with $\sigma_{\text{CCSN}} = 265 \text{ km s}^{-1}$ and predicts a reasonable local merger rate density for coalescing NSBHs and mass-gap NSBHs. A lower kick of $\sigma_{\text{CCSN}} = 61.6 \text{ km s}^{-1}$, obtained from NS binary systems without accounting for disrupted NSs, lead to an overly high merger rate.

We also show that the properties of the three NSBH merger events are consistent with our observable population. The isolated binary evolution channel predicts low BH spins in general. As a result, assuming it formed through the isolated binary evolution channel, the primary star mass of GW230529 can be well constrained to be located within the lower mass gap at the higher end. Moreover, the detection of GW230529 leads to an increase in the EMC fraction of coalescing NSBHs predicted by population models, as light BHs and NSs are easier to result in tidal disruption.

Our study has illustrated that coalescing NSBH population is valuable for understanding SN mechanisms, CE evolution, and

NS physics. Future detections of NSBH merger events could reveal whether the NS birth mass is limited, provide insights into SN remnant mass prescriptions, and further put constraints on CE efficiency and NS equations of state.

Acknowledgements. This work was supported by the Swiss National Science Foundation (project number PP00P2_211006). The POSYDON project is supported primarily by two sources: the Swiss National Science Foundation (PI Fragos, project numbers PP00P2_211006 and CRSII5_213497) and the Gordon and Betty Moore Foundation (PI Kalogera, grant award GBMF8477). Z.X. acknowledges support from the China Scholarship Council (CSC). E.Z. acknowledges funding support from the Hellenic Foundation for Research and Innovation (H.F.R.I.) under the "3rd Call for H.F.R.I. Research Projects to support Post-Doctoral Researchers" (Project No: 7933). M.B. acknowledges support from the Boninchi Foundation. K.A.R. is also supported by the Riedel Family Fellowship and thanks the LSSTC Data Science Fellowship Program, which is funded by LSSTC, NSF Cybertraining Grant No. 1829740, the Brinson Foundation, and the Moore Foundation; their participation in the program has benefited this work. K.K. acknowledges support from the Spanish State Research Agency, through the María de Maeztu Program for Centers and Units of Excellence in R&D, No. CEX2020-001058-M. J.J.A. acknowledges support for Program number (JWST-AR-04369.001-A) provided through a grant from the STScI under NASA contract NAS5-03127.

References

- Abac, A. G., Abbott, R., Abouelfettouh, I., et al. 2024, *ApJ*, 970, L34
- Abbott, B. P., Abbott, R., Abbott, T. D., et al. 2020a, *ApJ*, 892, L3
- Abbott, B. P., Abbott, R., Abbott, T. D., et al. 2020b, *Living Reviews in Relativity*, 23, 3
- Abbott, R., Abbott, T. D., Abraham, S., et al. 2021a, *ApJ*, 915, L5
- Abbott, R., Abbott, T. D., Abraham, S., et al. 2021b, *ApJ*, 923, 14
- Abbott, R., Abbott, T. D., Abraham, S., et al. 2020c, *ApJ*, 896, L44
- Abbott, R., Abbott, T. D., Acernese, F., et al. 2023, *Physical Review X*, 13, 041039
- Abbott, R., Abbott, T. D., Acernese, F., et al. 2024, *Phys. Rev. D*, 109, 022001
- Andrews, J., Bavera, S., Briel, M., et al. in prep.
- Bailyn, C. D., Jain, R. K., Coppi, P., & Orosz, J. A. 1998, *ApJ*, 499, 367
- Bavera, S. S., Fragos, T., Zapartas, E., et al. 2022, *A&A*, 657, L8
- Bavera, S. S., Fragos, T., Zevin, M., et al. 2021, *A&A*, 647, A153
- Broekgaarden, F. S., Berger, E., Neijssel, C. J., et al. 2021, *MNRAS*, 508, 5028
- Casares, J., Muñoz-Darias, T., Torres, M. A. P., et al. 2022, *MNRAS*, 516, 2023
- de Kool, M., van den Heuvel, E. P. J., & Pylyser, E. 1987, *A&A*, 183, 47
- Dewi, J. D. M. & Tauris, T. M. 2000, *A&A*, 360, 1043
- Falanga, M., Bozzo, E., Lutovinov, A., et al. 2015, *A&A*, 577, A130
- Farr, W. M., Sravan, N., Cantrell, A., et al. 2011, *ApJ*, 741, 103
- Fonseca, E., Cromartie, H. T., Pennucci, T. T., et al. 2021, *ApJ*, 915, L12
- Foucart, F., Hinderer, T., & Nissanke, S. 2018, *Phys. Rev. D*, 98, 081501
- Fragos, T., Andrews, J. J., Bavera, S. S., et al. 2023, *ApJS*, 264, 45
- Fryer, C. L., Belczynski, K., Wiktorowicz, G., et al. 2012, *ApJ*, 749, 91
- Godzieba, D. A., Radice, D., & Bernuzzi, S. 2021, *ApJ*, 908, 122
- Heida, M., Jonker, P. G., Torres, M. A. P., & Chiavassa, A. 2017, *ApJ*, 846, 132
- Hobbs, G., Lorimer, D. R., Lyne, A. G., & Kramer, M. 2005, *MNRAS*, 360, 974
- Jermyn, A. S., Bauer, E. B., Schwab, J., et al. 2023, *ApJS*, 265, 15
- Kalogera, V. & Baym, G. 1996, *ApJ*, 470, L61
- Kandel, D. & Romani, R. W. 2020, *ApJ*, 892, 101
- Kroupa, P. 2001, *MNRAS*, 322, 231
- Kruckow, M. U., Tauris, T. M., Langer, N., Kramer, M., & Izzard, R. G. 2018, *MNRAS*, 481, 1908
- Linares, M., Shahbaz, T., & Casares, J. 2018, *ApJ*, 859, 54
- Liotine, C., Kalogera, V., Briel, M., et al. in prep.
- Livio, M. & Soker, N. 1988, *ApJ*, 329, 764
- Mandel, I. & Smith, R. J. E. 2021, *ApJ*, 922, L14
- Nelson, D., Springel, V., Pillepich, A., et al. 2019, *Computational Astrophysics and Cosmology*, 6, 2
- O'Doherty, T. N., Bahramian, A., Miller-Jones, J. C. A., et al. 2023, *MNRAS*, 521, 2504
- Özel, F., Psaltis, D., Narayan, R., & McClintock, J. E. 2010, *ApJ*, 725, 1918
- Paxton, B., Bildsten, L., Dotter, A., et al. 2011, *ApJS*, 192, 3
- Paxton, B., Cantiello, M., Arras, P., et al. 2013, *ApJS*, 208, 4
- Paxton, B., Marchant, P., Schwab, J., et al. 2015, *ApJS*, 220, 15
- Paxton, B., Schwab, J., Bauer, E. B., et al. 2018, *ApJS*, 234, 34
- Paxton, B., Smolec, R., Schwab, J., et al. 2019, *ApJS*, 243, 10
- Podsiadlowski, P., Langer, N., Poelarends, A. J. T., et al. 2004, *ApJ*, 612, 1044
- Rhoades, C. E. & Ruffini, R. 1974, *Phys. Rev. Lett.*, 32, 324
- Román-Garza, J., Bavera, S. S., Fragos, T., et al. 2021, *ApJ*, 912, L23
- Romani, R. W., Kandel, D., Filippenko, A. V., Brink, T. G., & Zheng, W. 2021, *ApJ*, 908, L46
- Romani, R. W., Kandel, D., Filippenko, A. V., Brink, T. G., & Zheng, W. 2022, *ApJ*, 934, L17
- Sana, H., de Koter, A., de Mink, S. E., et al. 2013, *A&A*, 550, A107
- Shao, Y. & Li, X.-D. 2021, *ApJ*, 920, 81
- Siegel, J. C., Kiato, I., Kalogera, V., et al. 2023, *ApJ*, 954, 212
- Thompson, T. A., Kochanek, C. S., Stanek, K. Z., et al. 2019, *Science*, 366, 637
- Webbink, R. F. 1984, *ApJ*, 277, 355
- Xing, Z., Bavera, S. S., Fragos, T., et al. 2024, *A&A*, 683, A144
- Zdziarski, A. A., Mikolajewska, J., & Belczynski, K. 2013, *MNRAS*, 429, L104
- Zhu, J.-P., Hu, R.-C., Kang, Y., et al. 2024, *arXiv e-prints*, arXiv:2404.10596